

Battery cycle life study through relaxation and forecasting the lifetime via machine learning

Md Sazzad Hosen ^{a,*}, Rekabra Youssef ^a, Theodoros Kalogiannis ^a, Joeri Van Mierlo ^a, Maitane Berecibar ^a

^a Battery Innovation Center, MOBI Research Group, Vrije Universiteit Brussel, Pleinlaan 2, 1050, Brussels, Belgium



ARTICLE INFO

Keywords:
Relaxation study
Battery lifetime
Aging modeling
Machine learning
Gaussian process
Real-life validation

ABSTRACT

Battery lifetime modeling and prediction of precise capacity degradation for real-life applications are critical to understanding the complex and non-linear battery behavior. However, the application of accurate and robust aging models on dynamic on-road scenarios is still a challenge. In this work, a comprehensive aging dataset of 40 Nickel Manganese Cobalt (NMC) cells is generated for two years considering distinct relaxation phases in the function of the state of charge (SoC), temperature, and time. A qualitative analysis of the diversified aging parameters along with the sensitivity analysis of the rest criteria is conducted. Taking the discharge capacity as the pivotal predictor, a robust training dataset is built and preliminary fed to common data-driven models. Among them, the Gaussian process regression (GPR) is identified to be the best suit with which a 0.02% root-mean-squared error (RMSE) can be achieved for battery life prediction when tested with a static profile choosing an exponential kernel. Further, to demonstrate a real-life scenario, a worldwide harmonized light-duty test cycle (WLTC) is performed, and the capacity fade percentile can be predicted accurately with a 0.05% RMSE. This research shows that data-driven algorithms like GPR can be a promising online tool that can forecast the entire lifetime with high precision for dynamic profiles.

1. Introduction

Lithium-ion batteries' widespread use in present days has made them an integral part of our daily business thanks to their improved energy and power capabilities [1–3]. Especially, the automotive sector is highly motivated to deploy large-scale batteries in electric and hybrid electric vehicles (EV, HEV) [4], yet the challenge of precise lifetime prediction remains unresolved. The highly non-linear battery aging behavior and the cross-dependency of degradation parameters make the lifetime prediction further complex and difficult [5,6]. Thus, outlining the capacity fade during a lifetime needs a comprehensive analytical investigation and the outcome should be known to end-users to avoid unexpected situations. Hence, application-based diversified real scenarios are often non-reproducible in lab-level aging characterization which is critical to model development. An accurate and robust lifetime modeling approach holds immense importance which can replicate realistic scenarios.

It is a well-known fact in the present day that while on road, battery EVs not only undergo varying charge-discharge cycling processes but

also experience relaxation due to traffic or parking. Both phenomena are crucial as they happen at the same time while cycling and contribute to capacity degradation if not equally [7]. Thus, in this work, multiple relaxation phases are designed to perform via a lab-level extensive aging test program along with several cycling charge-discharge rates (C-rates) and at different operating temperatures (from 10°C to 45°C). The imposed rest phases somehow correspond to real-life scenarios. The impact of relaxation periods on lifetime plays a key role in the development of accurate aging models as well which often gets ignored in predictive approaches [8,9]. Several rest phases in terms of storage SoC, rest temperature, and rest time are used together with cycling operating conditions. The relaxation study investigated in this research has never been published on such a broader scale to the best knowledge of the authors.

However, with or without the consideration of breaks between aging tests, researchers have modeled the lifetime following several methodologies. Starting with a diverse electrochemical approach such as solid-electrolyte interface (SEI) [10,11], Li-plating [12], loss of active material [13], and impedance change [14], etc. have been considered

* Corresponding author.

E-mail address: md.sazzad.hosen@vub.be (M.S. Hosen).

separately to identify the degradation mechanisms. Although this approach may accurately define the degradation path, the increased complexity, and the interconnection of the mechanisms make it further complicated to deploy on a broader scale. Thus, semi-empirical approaches [7,15] have gained popularity where extensive lab-level data is generated to be fitted with crucial degradation factors such as depth of discharge (DoD) [16], temperature [17], ampere-hour throughput [18], SoC, and C-rates [19], modeling the lifetime in terms of capacity fade and/or power fade [20]. However, the accuracy is compromised against model complexity while limiting the target model application because the constructed models cannot be considered as technology-neutral. On the contrary, data-driven models that are performance-based have recently drawn serious attraction in battery state of health estimation (SoH) [21,22], remaining useful life (RUL) [23] and lifetime prediction [24,25] thanks to their high accuracy and less complex structure. Another crucial advantage of data-driven approaches is that the models can work to predict the battery life without any prior physical knowledge of the system. Thus, the trained models based on historical data can simulate the unknown operating inputs at a very high speed to provide an online output response. Machine learning (ML) algorithms such as support vector machine (SVM) [26,27], Gaussian process regression (GPR) [28,29], ensemble trees (EnsT) [30] etc. have frequently been used in battery health prognosis. Regardless, contrary to the estimation techniques, a substantial and high-quality battery cell aging database is the foremost part of any data-driven lifetime modeling approach which essentially defines the model robustness [24]. This may refer to the diversified aging parameters and/or interrelated sensor measurement formulating the targeted features for ML models [23,31]. Hence, the model adaptability and accuracy to the dynamic real-life operating conditions constructed from a specific set of performance-based inputs remain a challenge.

In this research, the authors have carefully designed and formulated a proof of concept to develop a lifetime model by choosing an ML approach that can be validated based on a real-life exercise. First, a rich aging database of 40 NMC cells is generated emulating a realistic battery test setup by cycling and relaxing the battery cells following the unique characterization and test plan explained in [Section 2](#). The sensitivity of the cycling aging and the relaxation parameters are then thoroughly analyzed in [Section 3](#) which led to the feature selection process. [Section 4](#) includes several ML algorithm results that are processed and trained with the generated dataset and the most suitable method is selected for model evaluation. A novel methodology of static and real-life profile testing is done in [Section 5](#) rationalizing the model's robustness. In the end, [Section 6](#) concludes the research achievement opening some future work aspects.

2. Methodology

For this research work, commercial high-energy pouch-shaped NMC cells are used to investigate within the whole test program framework. The discharged capacity of these cells varies between 59–62 Ah at room temperature. A series of special concepts were outlined for the entire campaign discussed in the following sub-sections.

2.1. Mechanical set up

All the investigated cells were mechanically sandwiched by metal plates to emulate realistic scenarios in an actual battery pack. [Fig. 1](#) clearly illustrates the designed setup where six bolts hold the plates and the cell on a Plexi-tray with an adjusted low torque of 0.4Nm. This constrained frame rigidly supports the cell which can result slightly in improved performance [32,33] and can support in terms of safety as well. For electrical attachment, dedicated low resistive metal blocks were used to ensure a strong connection.

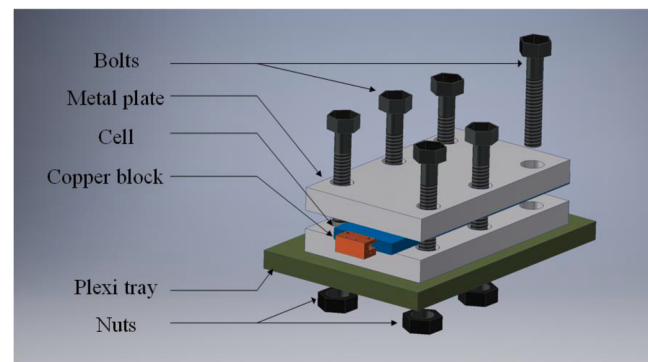


Fig. 1. Physical test setup of each investigated cell.

2.2. Experimental scheme

The structured test program starts with an initial pre-checkup of all the cells characterizing them at the beginning of life (BoL). It consists of two basic tests (capacity check and pulse test) at room temperature to identify the reference discharged capacity of the cells and the internal resistance (IR). The capacity check follows four constant-current and constant-voltage (CCCV) cycles at reference C/3 rate over the full operating voltage range and C/20 rate in the CV phase. On the other hand, the internal resistance measurement was done at three SoC points (80%, 50%, and 20%) following full CCCV charge and C/3 discharge to the target SoC. The IR calculation was done by imposing a 150A current pulse both towards charge and discharge directions for 10 seconds. A regular 30-minute rest was maintained between any charge and discharge step and a 10-minute rest amidst charge-discharge pulses. The SoH of the cell in terms of capacity and IR percentile is termed as the following basic equation.

$$\text{SoH} = \frac{\text{Actual capacity or IR}}{\text{BoL capacity or IR}} * 100 \% \quad (1)$$

After the BoL characterization, it was easily identified that the cells have reproducible results which are shown in [Fig. 2 \(a\)](#). Thus, the cells were categorized to perform single cycling mixed with relaxation condition apiece.

2.3. Relaxation Methodology

The aging test matrix including the relaxation phases can be outlined in [Fig. 2 \(b\)](#). Several aging conditions including charge-discharge rates varying from 0.33C to 2C and cycling temperatures from 10°C to 45°C were selected along with the relaxation phases in terms of rest temperatures (10°C to 45°C), rest SoCs (30%, 70%, 100%) and rest times (0.1 days to 10 days). All the cycle life tests were performed by the CCCV charge procedure and CC discharge method within the full voltage range explained in [Section 2.2](#). A 10-minute rest is induced in between every charge and discharge cycle. Ideally, 50 cycles per round format are followed before taking the cell to the rest phase uninterruptedly and by adjusting the rest SoC and temperature, accordingly. After completing the required relaxation, cells were then transferred back to cycling, continuing the rounds until they reach the end of life (EoL). Reaching an EoL of 75% SoH is marked as the end criterion for this work. The number of full cycles (100% DoD cycling) is considered as the cycle counter and the SoH is carefully monitored by adjusting [Eq. \(1\)](#) as [Eq. \(2\)](#). In this way, the capacity degradation analysis can avert potential negative fading due to voltage relaxation [34,35] and it essentially helps to construct a robust model.

$$\text{SoH}(\text{cell}\#) = \frac{\text{Last cycle discharge capacity per round}}{\text{Very first cycle discharge capacity}} * 100 \% \quad (2)$$

The complete cycling test program is performed with PEC ACT0550

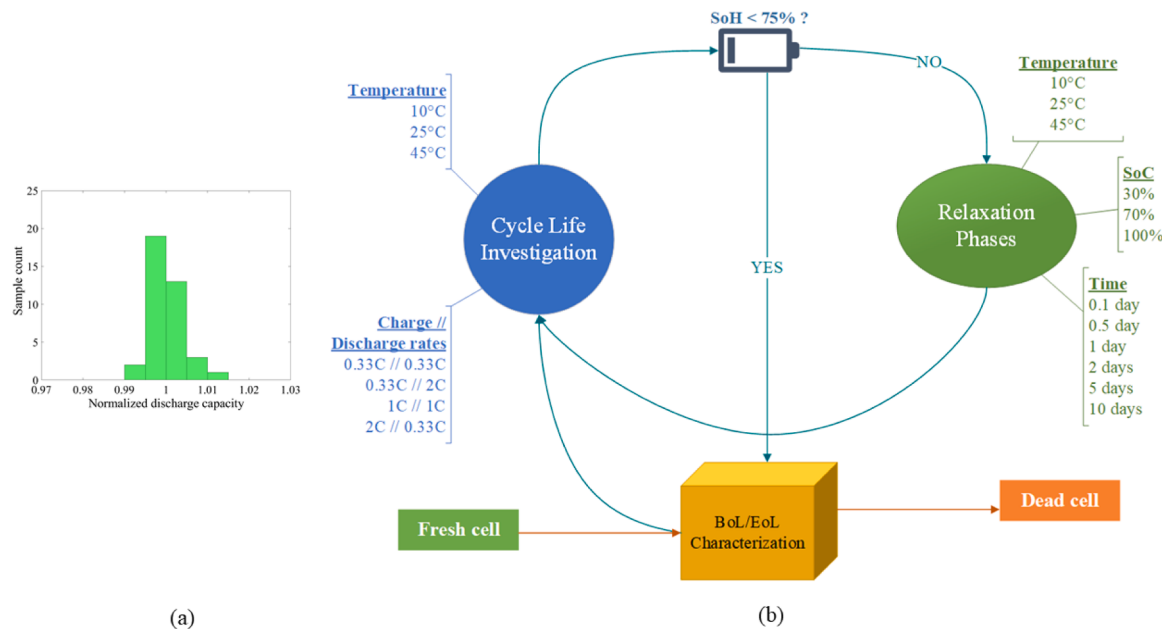


Fig. 2. (a) Normalized capacity histogram based on the mean value. (b) The designed aging test flow chart.

model testers and key measurements are recorded by built-in data loggers. To maintain specified cycling and relaxation temperature, CTS manufactured walk-in chambers and customized spacious climate rooms are used.

2.4. Model evaluation test plan

The research goal of this work is to develop a robust aging model based on the test matrix described in the previous Section 2.3. Thus, to validate the constructed model, a static CCCV and a realistic worldwide harmonized light-duty test cycle (WLTC) profile are designed and performed on separate cells. The static profile is an extension of the regular charge-discharge cycling followed in this study but in terms of longer-range rounds. A double round of each around 150 full cycles at 10° and with 1C charge-discharge rate condition is used relaxing the battery

at room temperature and 30% SoC for 1 day after the first round.

On the contrary, a dynamic cycling profile as WLTC is performed because it mirrors on-road driving and is derived from real data [36]. The following equation is used to design the WLTC profile based on a specific use case. In this work, the speed profile is calculated from the available public data and optimized for AUDI e-tron.

$$\text{WLTC}, I = \frac{\frac{1}{2} * \rho * S * \zeta * v^3 + \varphi * m * g * v + m * \alpha * v}{\eta * V} \quad (3)$$

In Eq. (3), $m = 2490$ kg (vehicle weight), $V = 396$ V (battery pack voltage), and the rest of the parameters are considered from common estimations such as $\rho = 1.2$ kg/m³ (air density), $S = 2$ m (frontal area), $\zeta = 0.32$ (co-efficient), $v = \text{velocity}$, $\phi = 0.01$ (co-efficient), $g = 9.8$ m/s² (gravity), $a = \text{acceleration}$, $\eta = 0.9$ (efficiency).

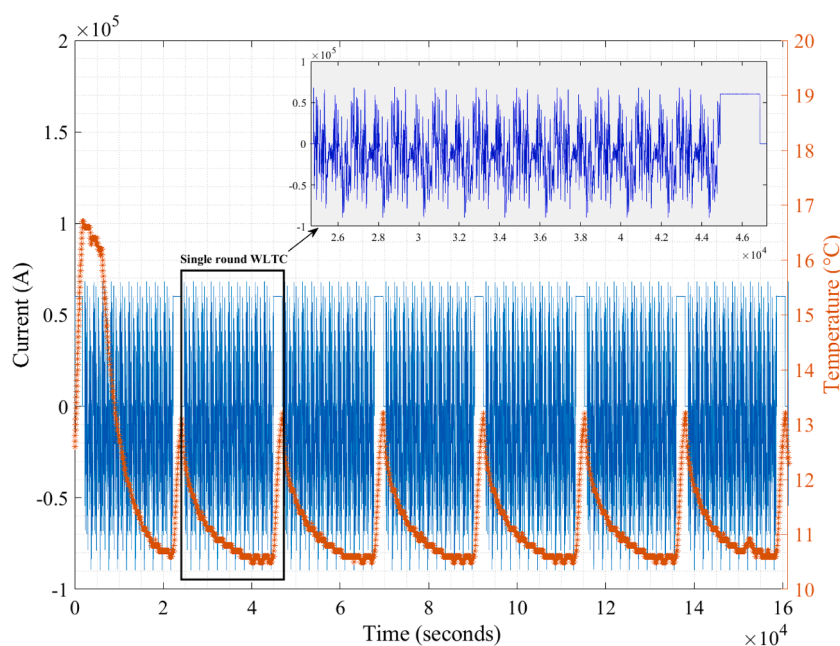


Fig. 3. Partial WLTC (sub-urban only) plot based on a real scenario.

For this work, only the sub-urban part of WLTC currents is used which is then adjusted to the cell level and is cycled continuously (10 times) in the SoC range of 95%-15% (80% operating window) as a single round before charging (CC) to the upper SoC start point. Several similar rounds of WLTCs were continued for 12 days (Fig. 3) and then the cell was rested with 70% SoC and at room temperature for 2 days. For cycling WLTC currents, 10°C was chosen to imitate the yearly mean temperature of Brussels, Belgium (10.3°C [37]). Unlike the static characterization between cycling rounds, a regular capacity (3 cycles with C/2 rate), and internal resistance (150A pulse current for 10 seconds at 50% SoC) checkups were done every 2 weeks (14 days of cycling and relaxation round). Both the profile types were tested under the same constrained setup until they reach EoL.

3. Relaxation results and impact on cycle life

The degradation mechanism in different Li-ion technologies has been well reported in the literature where multiple factors are identified as the root cause [5,6,38]. The crucial operation-specific stress parameters along with the interdependency of those factors result in a combined contribution in battery aging. Besides, the two main forms of the lifetime, typically reported as cycle life (in operation) and calendar life (storage or relaxation) are also interconnected especially while on-road which makes the degradation study further complicated [7,15]. Thus, the lithium battery aging understanding is quite a challenging task that requires extensive investigation corresponding to the electrochemical interpretation. Although the main purpose of this study is to focus on the impact of relaxation, the cycle of life aging could be analyzed as well.

3.1. Cycle life aging sensitivity analysis

The deterioration of the cycling capacity is related mainly to the charge-discharge parameters and the operating conditions. In this work,

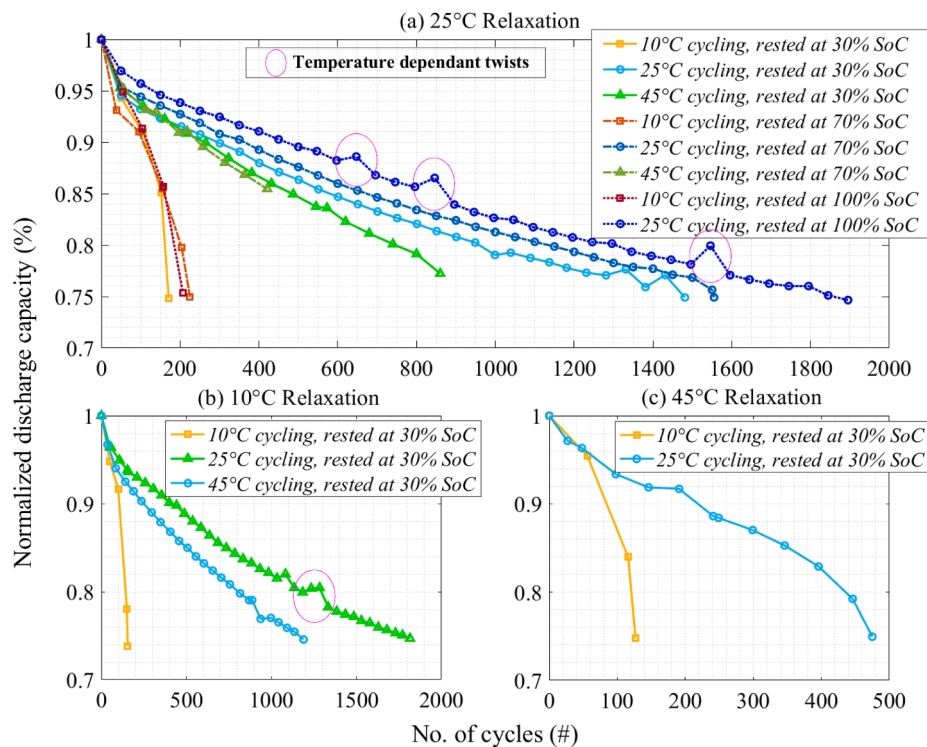
the cells are cycled with 100% DoD varying the intercalation and deintercalation speed at cold, moderate, and hot temperatures. Also, several relaxation phases are imposed which limit the findings when compared within similar boundary conditions. However, Fig. 4 can exhibit various non-identical cycling conditions capacity fade result at different rest SoCs and temperatures.

When the cells are cycled with a 1C rate continuously and rested for 5 days at room temperature then the cycling temperature clearly shows its dependency on the capacity fade. Low temperature (10°C) cycling has experienced the fastest degradation while 25°C cyclings can complete more than 1500 cycles. The active degradation mechanisms that happened in these cells at low temperature can be directly linked to lithium plating (for low temperature) and electrolyte decomposition, solid electrolyte interphase formation (SEI) growth (for high temperature), etc. [38]. The sharp steep in the degradation curves of 10°C cycling scenarios, especially, can also be linked to the imposed pressure but could not be verified. Fig. 4 (a) can also show the rest SoC dependency at room temperature cycling. Resting the battery cell at a fully charged state (at 100% SoC) has performed a larger number of cycles (28% higher compared to 30% SoC) meaning an extended lifetime in this case. However, rest SoC dependency at low and high-temperature cycling could not be distinguished clearly.

Similarly, Fig. 4 (a) and (b) display the same strong cycling temperature dependency when rested at 30% SoC irrespective of relaxation temperature. All the results explain that if a systematic test strategy is followed then for NMC cells, cycling at 10°C can seriously limit the lifetime. This also means that the faster degradation caused by lithium plating in NMC cells is much more powerful than other degradation mechanisms such as SEI growth and/or electrolyte decomposition etc.

3.2. Impact of relaxation phases on lifetime

There are two types of relaxation or rest periods that can be imposed



*Charge-discharge rate is denoted by '||'

Fig. 4. Capacity degradation (following Eq. (2)) of different cycling scenarios with 1C//1C rate and relaxed for 5 days after every round; (a) room temperature relaxation at various rest SoC, (b) 10°C relaxation at 30% SoC and (c) 45°C relaxation at 30% SoC. *Charge-discharge rate is denoted by '||'

during any cycling aging test. Like the first type, a regular 10-min rest in between charge and discharge steps is followed throughout the campaign concentrating more on the relaxation between cycling rounds. The other type allows the battery to rest after a certain period of cycling and this form of the rest is more identical to calendar life investigation, thus, the hybrid test methodology used in this work is closer to realistic scenarios such as driving on road and parking, etc. During the relaxation phases, the temperature, SoC, and the timespan are maintained carefully leaving off any unnecessary spells improving data quality. The sensitivity analysis of the relaxation parameters is analyzed separately to understand their impact on the lifetime.

3.3. Relaxation temperature dependency

The temperature being a critical parameter for ion-equalization during the diffusion process, may impact the capacity recovery. However, in this research, the capacity degradation in the long-term aging trend is investigated and the temperature dependency of the total lifetime is analyzed. Fig. 5 demonstrates the aging effects associated with low to high-temperature relaxation at 30% SoC compared to different cycling temperatures with a nominal 1C charge-discharge rate.

When the cells are cycled at 10°C and rested for 12 hours after every round, relaxing the cell at 45°C is found to be more damaging comparatively (Fig. 5 (a)). A similar trend is observed for 2-day and 5-day rests among the cells which may indicate certain electrochemical phenomena that are triggering the steep knee-shaped points. On the other hand, resting the cells for 0.5 days and 2 days at cold temperature, seem to have performed a larger number of cycles. Thus, it can be said that longer relaxation during 10°C does not necessarily increase the lifetime, however, the rest time dependency, in this case, is not clear and/or significant.

Likewise, the same significant high-temperature relaxation dependency can be seen in Fig. 5 (b) for 25°C cycling cells. The

insignificant rest temperature influence (at 10°C and 25°C) is also present both for at 25°C and 45°C cycling cells shown in Fig. 5 (b) and (c), respectively.

3.4. Relaxation SoC dependency

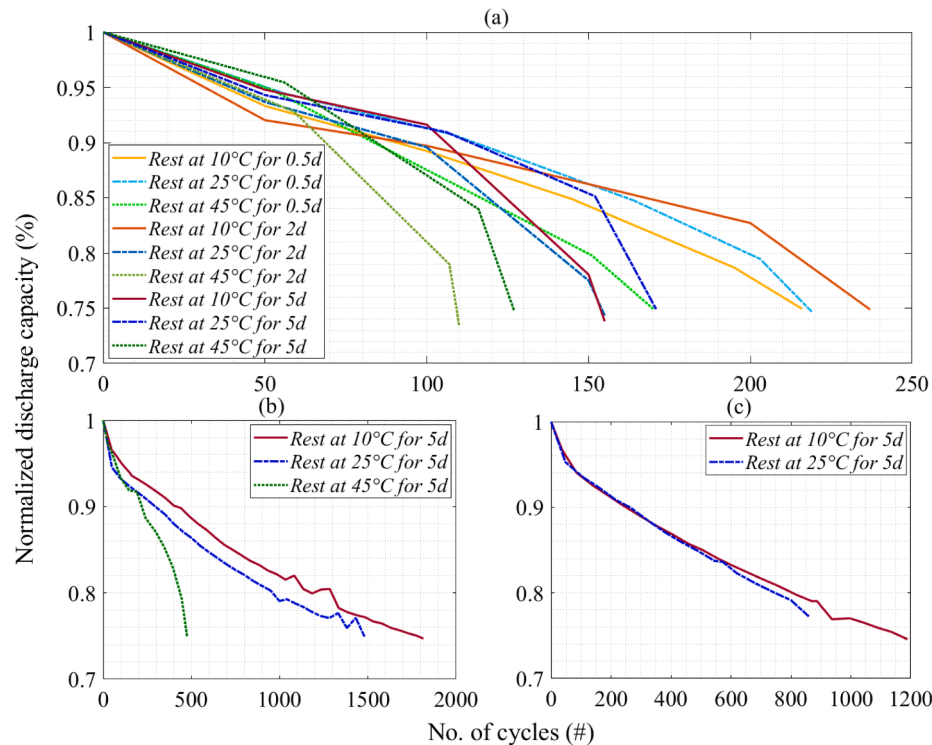
Capacity degradation at different relaxation SoCs for 5 days and at room temperature is compared in Fig. 6 (a-f) depending on different cycling conditions. For low-temperature cycling at 10°C, the rest SoC is found to have no clear effect on slow-rate cycling cells. While Fig. 6 (b) shows that 30% SoC is good for cells that are cycled with a high discharge rate, fast charging cells rested at 100% SoC seems to concede the fastest degradation. The striking difference can be seen between Fig. 6 (b) and (c) where the lithiation and de-lithiation speed have impacted the lifetime massively. Especially, cells cycling with fast charging have degraded rapidly only performing less than 20 cycles which points out the poor performance of the cell at this condition. Thus, Li-plating as one of the key degradation mechanisms at cold temperatures can be heavily linked to fast charging. However, 100% SoC relaxation has a higher negative influence on cell cycle life compared to lower SoC.

The cells cycled at 10°C, 25°C and 45°C with a nominal 1C charge-discharge rate have displayed no significant and/or clear SoC dependency (Fig. 6 (d-f)) when rested for 5 days.

3.5. Relaxation time dependency

The amount of time used to rest a cell in between cycling rounds, varies from hours to days (d). The investigated outcome is exhibited in Fig. 7 (a-f) by showing the relaxation time effect on aging. While plotting the comparisons only similar conditions are considered for better evaluation.

For low-temperature cycling of 10°C with a 1C rate, Fig. 7 (a-d)



*Charge-discharge rate is denoted by '||'

Fig. 5. Rest temperature influence of 1C//1C cycling scenarios when relaxed at 30% SoC after every round; (a) cycling at 10°C and relaxation at various temperatures, (b) 25°C cycling and 5 days rest and (c) 45°C cycling and 5 days rest. *Charge-discharge rate is denoted by '||'

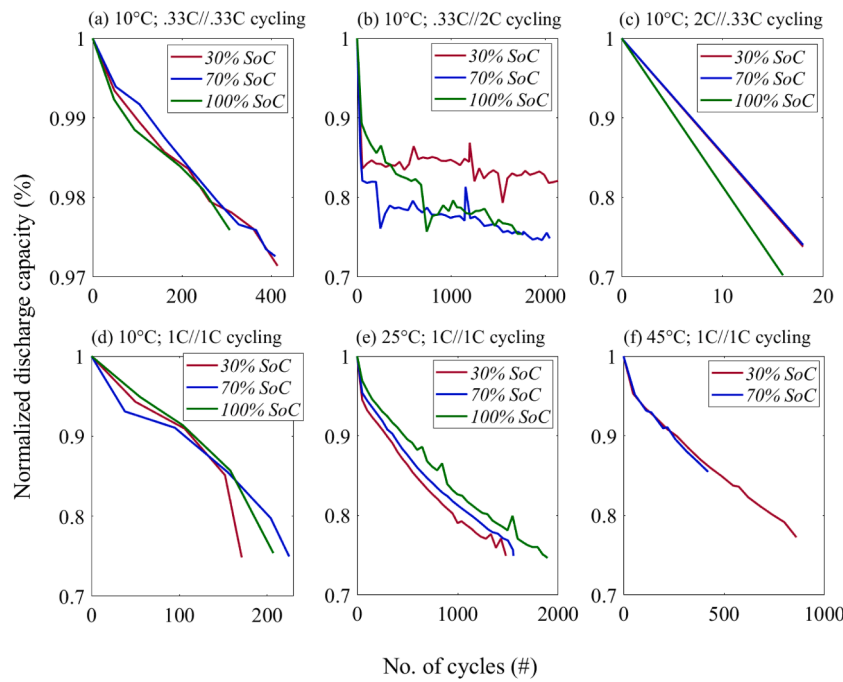
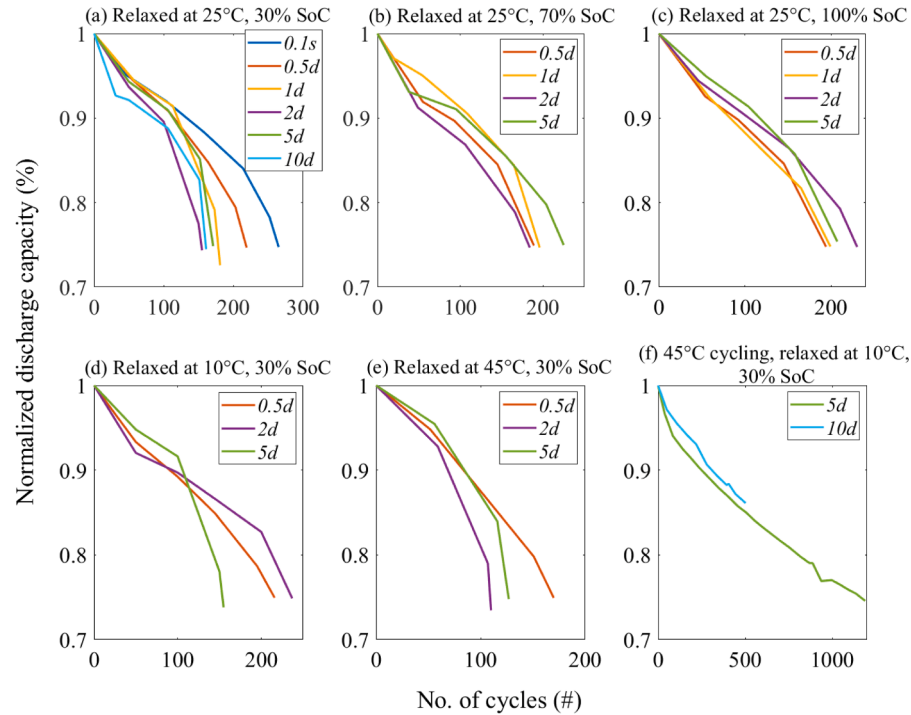


Fig. 6. Rest SoC influence of different cycling scenarios when relaxed at room temperature for 5 days after every round; (a-d) 10°C cycling with various charge-discharge rates as titled; In (a), note the vertical axis value, (e) 25°C cycling with nominal 1C//1C rate and (c) 45°C cycling with nominal 1C//1C rate. *Charge-discharge rate is denoted by ‘//’



*Charge-discharge rate is denoted by ‘//’

Fig. 7. Rest time influence of different cycling scenarios when relaxed at various temperature and SoC after every round; (a-c) 10°C cycling with 1C//1C rate relaxed at room temperature conditions as titled, (d) Same 10°C cycling relaxed at 10°C and 30% SoC, (e) Same 10°C cycling relaxed at 45°C and 30% SoC and (f) 45°C cycling with 1C//1C rate relaxed at conditions as titled. *Charge-discharge rate is denoted by ‘//’

describes the relaxation time impact for various rest temperatures and SoCs. When the cells are rested at room temperature and 30% SoC, shorter relaxation seems to have a better life. But relaxing at medium or full SoC, the difference in the performed number of cycles is

insignificant. However, no clear temperature dependency trend can be identified at any SoC for room temperature. Similarly, 10°C cycling cells relaxed at 10°C and 45°C and low SoC, do not exhibit a notable difference in aging.

On the other hand, the cells cycled at 45°C with a 1C rate and relaxed at 10°C and low SoC, show a similar aging trend for 5-day and 10-day rest. From the discussion so far, one can conclude that the impact of rest time on long-term cycling is trivial. It could not be stated that longer relaxation necessarily improves the lifetime, rather the calendar life capacity loss can add to the total degradation [7,15].

4. Data-driven model development

The comprehensive aging data generated in the framework of this research is associated with relaxation variables along with aging parameters. All these contributing factors are analyzed in Section 3 to identify the stressful parameters before feeding them to the model development process. In this work, several data-driven models are primarily trained with the generated high-quality dataset to select the best suit. The developed and optimized model is then validated with completely new cells for the whole lifetime proving robustness and applicability.

4.1. Data processing

In any data-driven modeling approach, the quality and the quantity of the data is the most crucial affair [23,39]. The utilized information can essentially impact model effectiveness if they are not consistent. The plentiful data produced in this work through one and a half years of investigation resulting in diverse aging curves displayed in Figs. 4 to 7. In this selected approach, the cell specification and/or path dependency declaration is unimportant. The interrelated aging mechanisms behind the non-linear degradation characteristics are attributed to several aging parameters. As the aging methodology used in this research is continuous and every relaxation during cycling is accounted, thus, each important parameter is recorded. It can also be mentioned here that every noise in the data can be connected to parameter variation related to either inconsistent temperature change or measurement issues. The latter is mostly linked to the temperature change during relaxation phases or regular equipment maintenance.

However, all the associated measured data are included in the data processing scheme taking every characteristic into primary consideration. Several Matlab scripts were built to extract, process, and organize aging data to construct the training bunch. This huge database includes aging parameters such as performed number of cycles, charge-discharge temperatures, and charge-discharge C-rates. It is also enriched with relaxation variables, for instance, rest temperatures and rest SoCs. As the rest time is found not to be an impactful parameter, thus, it is excluded from the training dataset. The output response is set as discharge capacity value after every cycle benchmarking the degradation scenario during the lifetime. Finally, the quality of the dataset is improved significantly by considering all but key specific parameters. Smoothing on any part of the dataset is ignored to avoid any misinterpretation of the interconnected aging variables.

So, the model considers seven inputs as cycle number, charge and discharge C-rates, charge and discharge temperatures, relaxation temperature and SoC. The output is quantified as the discharge capacity at every cycle associated with the input parameters. Moreover, testing data are also processed similarly and formatted according to the model input structure so that the actual measurement can be compared with the simulated capacity loss. In this case, the number of dynamic cycles is converted to the equivalent full cycle based on the nominal capacity making it similar to the input cycle count. Moreover, validation data are also processed similarly and adapted to make them comparable with the simulated capacity loss.

4.2. Primary selection of the model suitability

In this work, four different machine learning algorithms are primarily fitted with the processed single training dataset. This is to choose

the best fitting methodology before moving towards model development. These selected algorithms are ensemble-bagged trees, Gaussian process regression (GPR), support vector machine, and linear regression as these are the most common approaches in battery health prognosis. Other data-driven methods like artificial neural network (ANN), relevance vector machine (RVM), etc. are disregarded due to their complicated modeling structure. Matlab Regression Learner app is used for this preliminary selection by 5-fold cross-validation without any smoothing and tuning.

Ensembles of Trees: This type of decision tree means the combination of several weak learners by covering them up and improving the overall predictive performance. In this selection process, a bagged regression ensemble is used in which randomly selected predictions are averaged to make a robust output. This technique is useful when fewer training data is available such as in SoH and RUL estimations [30,40, 41].

Gaussian Process Regression: GPR is a kernel-based probabilistic machine learning technique that has recently gained attention in battery lifetime prognosis [25,29,42]. The Gaussian process is typically sensitive to inconsistent data (i.e., negative fade, noise, etc.) which is quite common in long-term non-linear aging. Thus, a suitable kernel or covariance function must be selected to get better modeling accuracy. During this selection, a simple exponential kernel is found to be explicit (Fig. 8 (b)) thanks to the excellent training data quality. So, a supervised tool like GPR can be very efficient if the kernel is selected appropriately with a consistent dataset.

Support vector machine: Like GPR, SVM is also a kernel-based approach, however, non-probabilistic meaning that the predictive parameters proportionally increase by the sample size. This makes SVM suitable for regression like continuous approach such as battery health estimation [43–45]. While choosing the best model, a fine Gaussian SVM is analyzed to fit the dataset.

Linear regression: A stepwise linear regression model is checked against the dataset for comparison's sake because the fitting of non-linear capacity degradation cannot be regulated with linear functions. The expected result can be seen in Fig. 8 (d) where response capacities form a considerable batch of outliers proving the unsuitability of this approach.

Four different metrics are used to evaluate the model performance supporting the best model choice. The errors are based on predicted capacity values compared to actual measurement [40].

$$\text{Root - mean - squared error (RMSE)} = \sqrt{\frac{1}{n} \sum_{i=1}^n (\bar{Y} - Y')^2} \quad (4)$$

$$\text{Mean - squared error (MSE)} = \frac{1}{n} \sum_{i=1}^n (\bar{Y} - Y')^2 \quad (5)$$

$$\text{Mean - absolute error (MAE)} = \frac{1}{n} \sum_{i=1}^n |\bar{Y} - Y'| \quad (6)$$

$$\text{The goodness of fit, } R^2 = 1 - \left[\sum_{i=1}^n (Y' - \bar{Y})^2 \Big/ \sum_{i=1}^n (Y' - Y)^2 \right] \quad (7)$$

In Eqs. (4), (5), (6), and (7), n is the number of samples, i denotes n number of iterations, \bar{Y} is the actual discharge capacity, Y is the mean of actual values and \bar{Y} is the model output response.

Among the evaluation metrics, RMSE is quite commonly used which compares the difference between the measured response to the predicted value putting weight into it. It can emphasize the deviation and assess the prediction performance. On the other hand, MSE as the squared-deviation average can also determine model efficiency and score, especially, considering unknown samples. MAE can be defined as the absolute and average error of all the predicted samples. Here, the identical weight of all the calculated errors means the prediction

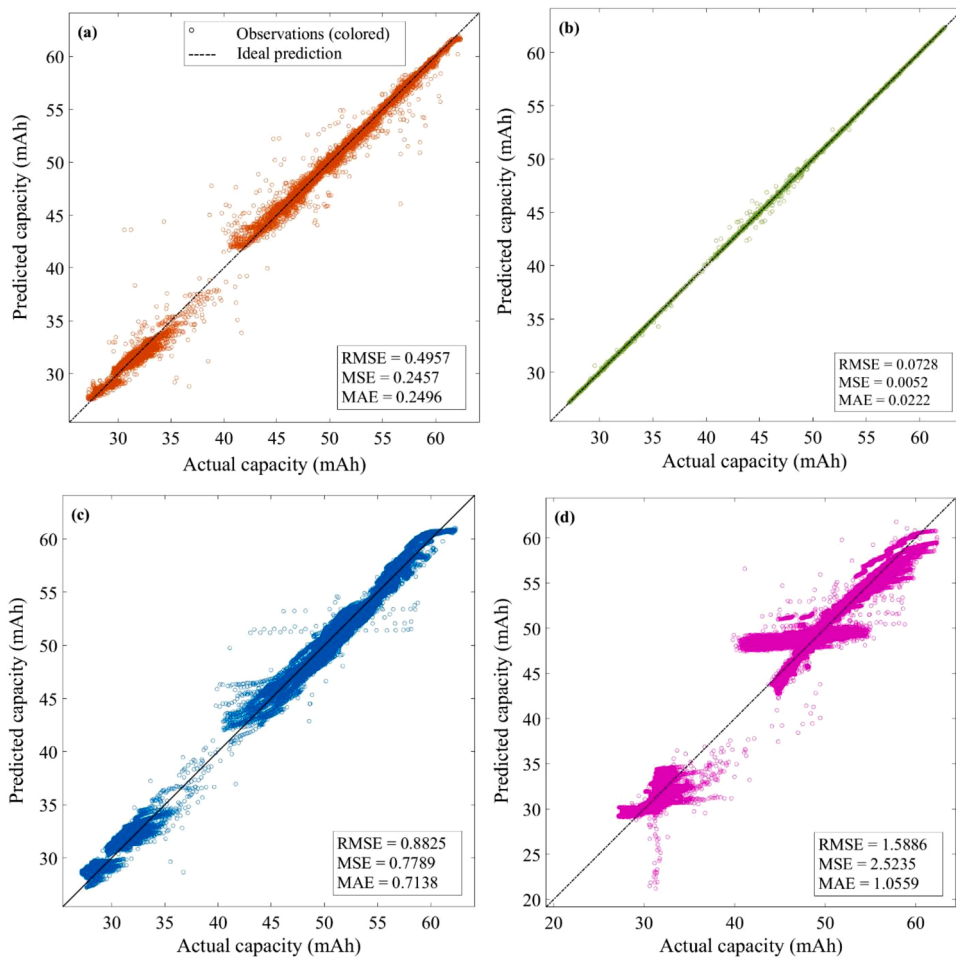


Fig. 8. Primary model selection by fitting the training data with (a) Ensemble-bagged tree, (b) Exponential GPR, (c) Fine-Gaussian SVM, and (d) Stepwise-linear regression.

accuracy corresponds to smaller MAE values. Finally, R-squared analyzes the regression model fit and can explain how well the actual data fit the predicted values. Several different metrics are used for comparing the model performances as there is no perfect fitting that exists. For evaluation purposes, the ideal RMSE value is the lower the better, MSE and MAE are good when the value is close to zero, and 1 is the best possible result for R^2 . In this study, 0.05% RMSE is targeted to achieve in the trained model testing stage using different unknown profiles.

After primary analysis of the training performance on the generated dataset, GPR is found to be the best-performed technique based on cross-validation with an RMSE value of 0.2956, MSE as 0.0874, MAE as 0.0831, and R^2 as 0.99 in capacity prediction. However, in terms of training duration, GPR took significant time taking 975.6 seconds compared to others all of which needed less than 38 seconds only. This notable training time can be compromised with the very high accuracy which other algorithms failed to achieve. The training of the models is conducted with Intel Core i7-6820HQ (at 2.70GHz) processor and 16GB (2133MHz speed). Fig. 8 (b) displays the excellent distribution of the trained data which drives the prediction accuracy showcasing the advantage of using the GPR approach. Further, the GPR model function is optimized in the next section by choosing different kernel functions to increase the robustness of the model. The trained GPR model is then used for the lifetime prediction on completely new cells both for long-run static and dynamic drive profiles.

4.3. Performance of the best model

The Gaussian process regression is identified to be the best-trained dataset in the previous section. GPR is a Bayesian-derived kernel-based non-parametric modeling technique that can be used for accurate battery degradation prediction [46].

The Gaussian process (GP) can be denoted as a probabilistic distribution function $f(x)$, in the relation with mean $m(x)$ and covariance $k(x, x^1)$ functions.

$$m(x) = \bar{E}(f(x)) \quad (8)$$

$$k(x, x^1) = \bar{E}[(f(x) - m(x)) * (f(x^1) - m(x^1))] \quad (9)$$

$$f(x) \sim GP(m(x), k(x, x^1)) \quad (10)$$

In Eqs. (8, 9 and 10), \bar{E} is the expected value but $m(x)$ is considered as a constant basis function set to zero. Thus, $k(x, x^1)$ kernel function explains the relevant difference between the predictive response and the true observation (actual capacity). GPR is a way of undertaking non-parametric regression by GP, where the crucial idea is to assume a sample Gaussian process function $f(x)$ instead of suggesting parametric function such as $f(x, \Theta)$ for Θ parameters estimation.

Being the covariance function or the kernel as the most critical aspect in GPR especially, there is no standardized but random selection process is followed which makes the choice process more challenging [47]. In this work, four different kernels are analyzed including the exponential kernel used in the preliminary model selection process. The residuals of

the simple exponential kernel are compared to other covariance functions named as matern 5/2, rational quadratic, and squared exponential. It is found that the trained GPR model by selecting exponential kernel following relative GPR equations exhibits the least residuals making it an obvious choice for the developed model optimization. Fig. 8 (b) exhibits how well the response capacities match with the actual values with GPR, however, the trained model needs to be able to predict the lifetime based on an unknown and finite collection of inputs. The data processing and the model script are developed using the Matlab platform.

5. Real application evaluation

The developed GPR model with the exponential kernel is optimized to simulate the validation profiles for the whole of their lifetime. The evaluation metrics from Eqs. (4–6) remain the same criteria to define the model's robustness and self-adaptive capability against unknown profiles.

5.1. Static profile validation

The trained GPR model is simulated by using the same input features but untrained (validation input parameters) for the static cycling profile that were used to train the model. The predicted aging starts right from the BoL till the performed number of cycles which is plotted in Fig. 9 (a) versus the measured degradation. The tested data structure follows the same seven parameters comprised of cycle number, charge-discharge temperature, C-rates and relaxation time, SoC etc. It can be seen that the model can predict the lifetime with very high accuracy (see Table 1 for evaluation). However, two unusual simulation scenarios are observed in Fig. 9 (a), one of which is a typical model glitch. This results in a sudden capacity increase in the simulation and can be referred to as temperature variation usually happens at times during measurement (see top inserted axis). Although the longer noise in temperature reflects in output capacity measurement too, the model sensitively misinterprets this sudden feature drop which may not be seen in the capacity observations. The other simulation scenario consists of overfitting in the beginning and underfitting after the intersection point. The zoomed-in bottom inserted axis shows that after finishing the first round and relaxation, the static profile has a capacity gain which the model could not predict referring to the GPR's limitation in predicting capacity regeneration [22,48].

Table 1

Model performance of the validation profiles based on normalized capacity fade percentile.

	Static profile	WLTC
RMSE	0.0159	0.0458
MSE	0.0003	0.0021
MAE	0.0151	0.0324

5.2. Dynamic WLTC demonstration

Furthermore, the developed model can predict the lifetime accurately of a real-life dynamic profile as explained in Section 2.4. Typically, on-road vehicles undergo many shallow charge-discharge cycles which eventually drain the battery before getting charged again. In this work, the 80% operating window or DoD cycling is thus adjusted in terms of the number of cycles to match the trained model input feature. In this case, a DoD factor is considered in a relation to achieving the corrected cycle numbers that are found with the cycled cell's internal resistance which sheds light on sudden degradation knee-points. The recorded charge and discharge mean temperature and C-rates at every round are used along with the relaxation temperature and SoC as imposed.

$$C_{adj} = k * C_{n-1} \left(1 + \sum_{i=1}^n IR \right) \quad (11)$$

In Eq. (11), C_{adj} is the adjusted number of cycles, k is the full DoD adjustment factor which is 1.3 (calculated against DoD Ah) in this work, C_{n-1} is performed WLTC numbers, and i denotes to n number of iteration rounds. The relationship can be realized in Fig. 9 (b) where the resistance growth especially towards the end of life, impacts the capacity drop. Machine learning algorithms can be used to predict these knee-points, however, it is a challenging task taking technology diversity and operating conditions variation into account [49].

Besides, to simulate the developed trained GPR model, the mean charge-discharge rate is used per round corresponding to the crucial features. Fig. 9 (b) shows that the measured capacity fade during the WLTC rounds is in excellent agreement with the adjusted number of cycles calculated based on cumulative internal resistance growth. Finally, it can be demonstrated that the optimized and simulated GPR model can precisely predict the capacity degradation which proves its robustness. Table 1 includes superb evaluation results. The simulated degradation curve could follow the measured capacity fade almost till the EoL until the steep bend in the capacity fade comes into effect possibly due to Li-plating resulting in higher IR growth. The model underfits the capacity drops during the last round referring to additional

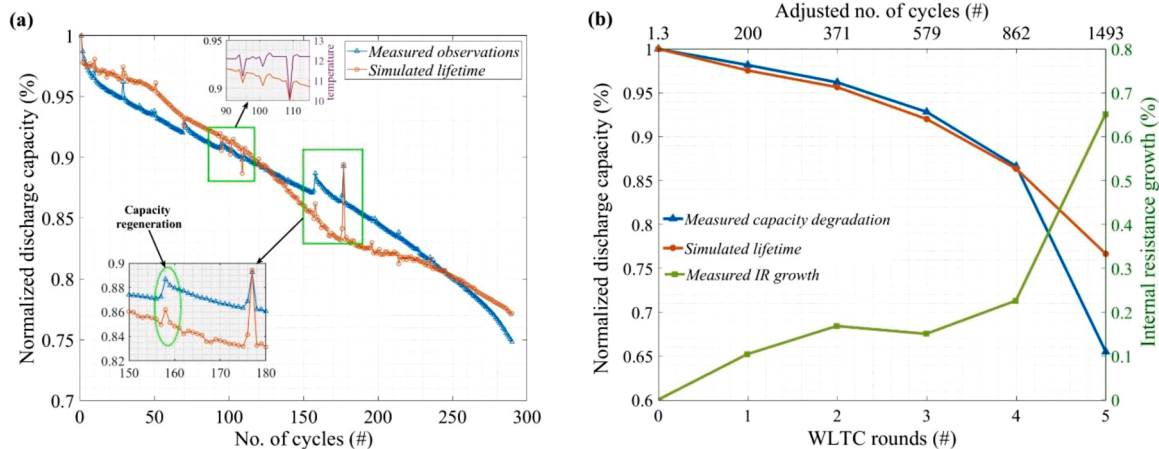


Fig. 9. Model testing against dynamic cycling; (a) degradation for a static profile where inserted axes refer to the model's sensitivity and GPR's limitation against regenerative capacity. (b) for a realistic WLTC profile capacity fade which is in connection with the internal resistance growth.

effective degradation mechanisms that become active during aging. Further, investigation on these sudden knee-points can be made in the future to improve the model reliability.

5.3. Rationalization of lifetime forecasting

The extensive study on battery cycling in this research supports both the qualitative degradation analysis and the quantitative feature selection to develop a robust lifetime model with the Gaussian process regression technique. The hybrid type test campaign allows investigating the sensitive degradation parameters which also define the model parameter selection. To the best of the authors' knowledge, such detailed modeling investigation generating a novel and high-quality dataset has not been performed before considering several ML techniques. The high-quality training dataset generated in this research is the key to develop a robust machine learning model. It is a very common practice to use a single-aging dataset both for training and testing purposes using ML methodologies which may question the developed model's suitability to real-life conditions, however, a few works have performed a proper model testing. Hence, model evaluation based on early predictions may also require a wide range of input parameters consideration that is a challenging task. In this research, an on-road vehicle profile is simulated and compared with observations from a completely new cell for the whole lifetime without retraining the model. The very high accuracy proves that this modeling tool can provide a one-fit-all solution. GPR can identify the degradation path based on lab investigation without prior knowledge of the battery technology. The novel testing plan can also be considered as complete as it includes both the aging forms (cycling and relaxation/storage) and the main output responses (capacity degradation and IR growth) throughout the lifetime. A functioning lifetime model such as the developed one can be utilized for lifetime prognosis based on any application profile using this cell. It would help the original equipment manufacturers (OEMs) to study the aging characteristics in detail and can take the necessary steps to further develop the cell's life cycle. However, unlike semi-empirical methods, the limitation of applying ML approaches would still exist such as separation of aging impacts by degradation parameters. The individual

Moreover, the trained GPR model can be used as an online-simulation tool to track the lifetime based on real dynamic driving profiles. Nothing but a short (10 seconds) pulse test would be required to simulate the model in real-time. The constructed model and the research work also make a breakthrough in establishing a relationship between WLTC cycles and the cell's internal resistance contributing to total capacity degradation. The research outcome can help to understand the reliability of a battery system cycled in on-road electric vehicles.

6. Conclusion

Data-driven models like GPR can be a promising solution in battery lifetime prediction supporting not only the battery design and development process but also in online aging forecasting. For this, the high-quality dataset generated in this research can identify the sensitive aging parameters and the relaxation impacts on cycle life. The processed dataset consisting of the crucial aging features is fitted with several ML models from which the GPR approach with exponential kernel gives the best results. The robust model can successfully predict a static profile with an RMSE of 0.02% and a realistic dynamic WLTC profile with only 0.05% RMSE. Such a high accurate data-driven model considering the key degradation features is rare in literature and a trade-off between the computational effort and model complexity. Although this approach requires a substantial study as a prerequisite, the developed model can be implemented for the online prognosis and diagnosis of the battery in a real vehicle. Moreover, the developed knowledge can help to understand the aging mechanisms of a complex system like Li-ion batteries by analyzing the stressful parameters individually.

In the future, aged battery cells can be further analyzed by post-

mortem analysis to identify crucial physical damages that resulted from this study. The excellent dataset can be used for other ML techniques such as artificial neural networks and semi-empirical methods and/or with a hybrid methodology to compare different aging modeling methodologies. Furthermore, the developed model can be tested for other Li-ion technologies by designing a similar lifetime investigation.

Author statement

Md Sazzad Hosen: Conceptualization, Methodology, Software, Validation, Investigation, Data Curation, Writing – Original Draft

Rekabra Youssef: Investigation, Data Curation, Validation

Theodoros Kalogiannis: Investigation, Data Curation, Visualization

Joeri Van Mierlo: Writing – Review & Editing

Maitane Berecibar: Supervision, Writing – Review & Editing

Declaration of Competing Interest

The authors declare that they have no known competing financial interests or personal relationships that could have appeared to influence the work reported in this paper.

Acknowledgment

The battery lifetime test campaign and the full work has been done in the Battery Innovation Center of MOBI Research Group. The project was financially supported by Vrije Universiteit Brussel.

References

- [1] B. Scrosati, J. Garche, Lithium batteries : status , prospects and future, 195 (2010) 2419–2430. doi:10.1016/j.jpowsour.2009.11.048.
- [2] B. Nykvist, M. Nilsson, Rapidly falling costs of battery packs for electric vehicles, 5 (2015) 100–103. doi:10.1038/NCLIMATE2564.
- [3] W. Waag, C. Fleischer, D. Uwe, Critical review of the methods for monitoring of lithium-ion batteries in electric and hybrid vehicles, *J. Power Sources*. 258 (2014) 321–339, <https://doi.org/10.1016/j.jpowsour.2014.02.064>.
- [4] A. Barré, B. Deguilhem, S. Grolleau, M. Gérard, F. Suard, D. Riu, A review on lithium-ion battery ageing mechanisms and estimations for automotive applications, *J. Power Sources* 241 (2013) 680–689, <https://doi.org/10.1016/j.jpowsour.2013.05.040>.
- [5] J. Vetter, P. Novák, M.R. Wagner, C. Veit, K.C. Moller, J.O. Besenhard, M. Winter, M. Wohlfahrt-Mehrens, C. Vogler, A. Hammouche, Ageing mechanisms in lithium-ion batteries, *J. Power Sources* (2005), <https://doi.org/10.1016/j.jpowsour.2005.01.006>.
- [6] M.R. Palatin, Understanding ageing in Li-ion batteries: a chemical issue, *Chem. Soc. Rev.* 47 (2018) 4924–4933, <https://doi.org/10.1039/C7CS00889a>.
- [7] S. Hosen, D. Karimi, T. Kalogiannis, A. Pirooz, Electro-aging model development of nickel-manganese-cobalt lithium-ion technology validated with light and heavy-duty real-life pro files, *J. Energy Storage* 28 (2020), 101265, <https://doi.org/10.1016/j.est.2020.101265>.
- [8] M. Reichert, D. Andre, A. Rössmann, P. Janssen, H. Bremes, D.U. Sauer, S. Passerini, M. Winter, In fl uence of relaxation time on the lifetime of commercial lithium-ion cells, *J. Power Sources* 239 (2013) 45–53, <https://doi.org/10.1016/j.jpowsour.2013.03.053>.
- [9] X. Xu, C. Yu, S. Tang, X. Sun, X. Si, Remaining Useful Life Prediction of Lithium-Ion Batteries Based on Wiener Processes with Considering the Relaxation Effect, 2019.
- [10] M.B. Pinson, M.Z. Bazant, J.E. Soc, P. A-a, M.B. Pinson, M.Z. Bazant, Theory of SEI formation in rechargeable batteries : capacity fade , accelerated aging and lifetime prediction service theory of sei formation in rechargeable batteries : capacity fade, Accelerated Aging Lifetime Prediction (2013) 160, <https://doi.org/10.1149/2.044302jes>.
- [11] J. Christensen, J. Newman, A mathematical model for the lithium-ion negative electrode solid electrolyte interphase, (2014) 1–2. doi:10.1149/1.1804812.
- [12] X. Yang, Y. Leng, G. Zhang, S. Ge, C. Wang, Modeling of lithium plating induced aging of lithium-ion batteries : transition from linear to nonlinear aging, *J. Power Sources* 360 (2017) 28–40, <https://doi.org/10.1016/j.jpowsour.2017.05.110>.
- [13] J. Christensen, J. Newman, Cyclable lithium and capacity loss in Li-ion cells, (2005) 818–829. doi:10.1149/1.1870752.
- [14] A. Maheshwari, M. Heck, M. Santarelli, Cycle aging studies of lithium nickel manganese cobalt oxide-based batteries using electrochemical impedance spectroscopy, *Electrochim. Acta* 273 (2018) 335–348, <https://doi.org/10.1016/j.electacta.2018.04.045>.
- [15] J. De Hoog, J. Timmermans, D. Ioan-stroe, M. Swierczynski, J. Jaguemont, S. Goutam, N. Omar, J. Van Mierlo, P. Van Den Bossche, Combined cycling and calendar capacity fade modeling of a Nickel-Manganese-Cobalt Oxide Cell with

- real-life profile validation, *Appl. Energy* 200 (2017) 47–61, <https://doi.org/10.1016/j.apenergy.2017.05.018>.
- [16] J. Schmalstieg, S. Käbitz, M. Ecker, D.U. Sauer, A holistic aging model for Li (NiMnCo)O₂ based 18650 lithium-ion batteries, *J. Power Sources* 257 (2014) 325–334, <https://doi.org/10.1016/j.jpowsour.2014.02.012>.
- [17] M. Ecker, N. Nieto, S. Käbitz, J. Schmalstieg, H. Blanke, A. Warnecke, D. Uwe, Calendar and cycle life study of Li (NiMnCo) O₂-based 18650 lithium-ion batteries, *J. Power Sources* 248 (2014) 839–851, <https://doi.org/10.1016/j.jpowsour.2013.09.143>.
- [18] I. Gandiaga, I. Villarreal, Cycle ageing analysis of a LiFePO₄/graphite cell with dynamic model validations : towards realistic lifetime predictions, *J. Power Sources* 275 (2015) 573–587, <https://doi.org/10.1016/j.jpowsour.2014.10.153>.
- [19] N. Omar, M. Abdel, Y. Firouz, J. Salminen, J. Smekens, O. Hegazy, H. Gaulous, G. Mulder, P. Van Den Bossche, T. Coosemans, Lithium iron phosphate based battery – assessment of the aging parameters and development of cycle life model, *Appl. Energy* 113 (2014) 1575–1585, <https://doi.org/10.1016/j.apenergy.2013.09.003>.
- [20] J. de Hoog, J. Jaguemont, A. Nikolian, J. Van Mierlo, P. Van Den Bossche, N. Omar, A combined thermo-electric resistance degradation model for nickel manganese cobalt oxide based lithium-ion cells, *Appl. Therm. Eng.* 135 (2018) 54–65, <https://doi.org/10.1016/j.applthermaleng.2018.02.044>.
- [21] M. Berecibar, I. Gandiaga, I. Villarreal, N. Omar, J. Van Mierlo, P. Van Den Bossche, Critical review of state of health estimation methods of Li-ion batteries for real applications, *Renew. Sustain. Energy Rev.* 56 (2016) 572–587, <https://doi.org/10.1016/j.rser.2015.11.042>.
- [22] Y. Li, K. Liu, A.M. Foley, A. Zülke, M. Berecibar, E. Nanini-maury, J. Van Mierlo, H. E. Hostler, Data-driven health estimation and lifetime prediction of lithium-ion batteries : a review, 113 (2019). doi:10.1016/j.rser.2019.109254.
- [23] X. Hu, L. Xu, X. Lin, M. Pecht, Battery Lifetime Prognostics, (2020) 1–37. doi: 10.1016/j.joule.2019.11.018.
- [24] K.A. Severson, P.M. Attia, N. Jin, N. Perkins, B. Jiang, Z. Yang, M.H. Chen, M. Aykol, P.K. Herring, D. Fragedakis, M.Z. Bazant, S.J. Harris, W.C. Chueh, R. D. Braatz, capacity degradation, *Nat. Energy* 4 (2019) 383–391, <https://doi.org/10.1038/s41560-019-0356-8>.
- [25] M. Lucu, E. Martinez-laserna, I. Gandiaga, K. Liu, H. Camblong, W.D. Widanage, Data-driven nonparametric Li-ion battery ageing model aiming at learning from real operation data - Part B : cycling operation, *J. Energy Storage* 30 (2020), 101410, <https://doi.org/10.1016/j.est.2020.101410>.
- [26] Q. Zhao, X. Qin, H. Zhao, W. Feng, A novel prediction method based on the support vector regression for the remaining useful life of lithium-ion batteries, *Microelectron. Reliab.* 85 (2018) 99–108, <https://doi.org/10.1016/j.micrel.2018.04.007>.
- [27] B. Gu, V.S. Sheng, K.Y. Tay, W. Romano, S. Li, for Ordinal Regression, 26 (2015) 1403–1416.
- [28] K. Liu, Y. Li, X. Hu, S. Member, Relevance Determination kernel for calendar aging prediction of lithium-ion batteries, 16 (2020) 3767–3777. doi:10.1109/TII.2019.2941747.
- [29] R.R. Richardson, M.A. Osborne, D.A. Howey, Gaussian process regression for forecasting battery state of health, *J. Power Sources* 357 (2017) 209–219, <https://doi.org/10.1016/j.jpowsour.2017.05.004>.
- [30] S. Khaleghi, Y. Firouz, M. Berecibar, J. Van Mierlo, P. Van Den Bossche, Ensemble Gradient Boosted Tree for SoH Estimation, (2020).
- [31] M. Lucu, I. Gandiaga, H. Camblong, Review article A critical review on self-adaptive Li-ion battery ageing models, 401 (2018) 85–101.
- [32] M. Wünsch, J. Kaufman, D. Uwe, Investigation of the influence of different bracing of automotive pouch cells on cyclic lifetime and impedance spectra, *J. Energy Storage* 21 (2019) 149–155, <https://doi.org/10.1016/j.est.2018.11.019>.
- [33] J. Cannarella, C.B. Arnold, Stress evolution and capacity fade in constrained lithium-ion pouch cells, *J. Power Sources* 245 (2014) 745–751, <https://doi.org/10.1016/j.jpowsour.2013.06.165>.
- [34] B. Epding, B. Rumberg, H. Jahnke, I. Stratmann, A. Kwade, Investigation of significant capacity recovery effects due to long rest periods during high current cyclic aging tests in automotive lithium ion cells and their influence on lifetime, *J. Energy Storage* 22 (2019) 249–256, <https://doi.org/10.1016/j.est.2019.02.015>.
- [35] M. Lewerenz, P. Dechen, D. Uwe, Investigation of capacity recovery during rest period at different states-of, *J. Energy Storage* 21 (2019) 680–690, <https://doi.org/10.1016/j.est.2019.01.004>.
- [36] M. Tutuianu, A. Marotta, H. Steven, E. Ericsson, T. Haniu, N. Ichikawa, H. Ishii, Development of a World-wide Worldwide harmonized Light duty driving Test Cycle (WLTC) ~ Technical Report ~ DHC subgroup, 03 (2014) 7–10.
- [37] Webpage, (2020). <https://en.climate-data.org/europe/belgium/brussels-capital/brussels-6316/> (accessed May 26, 2020).
- [38] C.R. Birk, M.R. Roberts, E. McTurk, P.G. Bruce, D.A. Howey, Degradation diagnostics for lithium ion cells, *J. Power Sources* 341 (2017) 373–386, <https://doi.org/10.1016/j.jpowsour.2016.12.011>.
- [39] M. Dubarry, D. Beck, Benchmark synthetic training data for artificial intelligence-based Li-ion diagnosis and prognosis, (2020) 1–20. doi:10.20944/preprints202005.0106.v1.
- [40] Y. Li, C. Zou, M. Berecibar, E. Nanini-maury, J.C. Chan, P. Van Den Bossche, J. Van Mierlo, N. Omar, Random forest regression for online capacity estimation of lithium-ion batteries, 232 (2018) 197–210. doi:10.1016/j.apenergy.2018.09.182.
- [41] Y. Xing, E.W.M. Ma, K. Tsui, M. Pecht, Microelectronics Reliability An ensemble model for predicting the remaining useful performance of lithium-ion batteries, *Microelectron. Reliab.* 53 (2013) 811–820, <https://doi.org/10.1016/j.micrel.2012.12.003>.
- [42] K. Liu, X. Hu, Z. Wei, Y. Li, Y. Jiang, Modified Gaussian process regression models for cyclic capacity prediction of, 7782 (2019). doi:10.1109/TTE.2019.2944802.
- [43] A. Nuhic, T. Terzimehic, T. Soczka-guth, M. Buchholz, K. Dietmayer, Health diagnosis and remaining useful life prognostics of lithium-ion batteries using data-driven methods q, *J. Power Sources* 239 (2013) 680–688, <https://doi.org/10.1016/j.jpowsour.2012.11.146>.
- [44] T. Qin, S. Zeng, J. Guo, Microelectronics Reliability Robust prognostics for state of health estimation of lithium-ion batteries based on an improved PSO – SVR model, *MR* 55 (2015) 1280–1284, <https://doi.org/10.1016/j.micrel.2015.06.133>.
- [45] D. Andre, C. Appel, T. Soczka-guth, D. Uwe, Advanced mathematical methods of SOC and SOH estimation for lithium-ion batteries, *J. Power Sources* 224 (2013) 20–27, <https://doi.org/10.1016/j.jpowsour.2012.10.001>.
- [46] C.E. Rasmussen, C.K.I. Williams, *G. Processes*, M.I.T. Press, M.I. Jordan, Gaussian processes for machine learning, 2006.
- [47] D. Duvenaud, J.R. Lloyd, R. Grosse, J.B. Tenenbaum, L. Lin, Structure discovery in nonparametric regression through compositional kernel search, 28 (2013).
- [48] D. Liu, J. Pang, J. Zhou, Y. Peng, M. Pecht, Microelectronics reliability Prognostics for state of health estimation of lithium-ion batteries based on combination Gaussian process functional regression, *Microelectron. Reliab.* 53 (2013) 832–839, <https://doi.org/10.1016/j.micrel.2013.03.010>.
- [49] P. Fermín-cueto, E. Mcturk, M. Allerhand, E. Medina-lopez, M.F. Anjos, J. Sylvester, Q. Court, H. Watt, Energy and AI Identification and machine learning prediction of knee-point and knee-onset in capacity degradation curves of lithium-ion cells, 1 (2020). doi:10.1016/j.egyai.2020.100006.